Weierstraß-Institut
für Angewandte Analysis und Stochastik

Self-pulsation and excitability of blue-violet InGaN lasers

V.Z.Tronciu[1], Minoru Yamada[2], R.A.Abram[3], Toshiyuki Kawakami[4],

Shigetoshi Ito[4], Tomoki Ohno[4], Mototaka Taneya[4]

submitted: 03.06.2004

[1] Department of Physics
     Technical University of Moldova
     Stefan cel Mare 168
     Chisinau MD-2004 Moldova
     E-Mail: tronciu@mail.utm.md

[2] Faculty of Engineering, Kanazawa
     University, 2-40-20, Kodatsuno,
     Kanazawa, 920-8667, Japan
     E-Mail: myamada@t.kanazawa-u.ac.jp

[3] Department of Physics,
     University of Durham,
     Durham DH1 3LE, UK
     E-Mail: R.A.Abram@durham.ac.uk

[4] The Devices Technology Research
     Laboratories, Sharp Corporation,
     Japan

W I A S

Abstract

This article gives a review of our latest results on the self-pulsation and excitability properties of blue-violet lasers. A number of investigations of the phenomena in InGaN lasers with different designs are described. The bifurcations, which are the origin of the phenomena, are identified and the effects of the lasers parameters on device dynamics are discussed. It is shown how different laser structures can be used to control device behaviour and the dependence of self-pulsation and excitability behaviour on laser geometry is discussed. Finally, agreement between the results of numerical calculations and experimental measurements on self-pulsation is demonstrated.

1 Introduction

Blue-violet semiconductor lasers are very attractive for high-density optical storage applications [1]. In particular, laser diodes operating at 400nm are required for CD or DVD systems to increase the disk storage capacity up to 25 Gbytes. A number of other applications, such as full colour electroluminescent displays, laser printers, detectors, sources for undersea communications, and many others in biology and medicine have increased the interest in such lasers. In recent years, numerous fabrication methods have been proposed and developed for blue lasers with CW operation. However, recently, specific interest has been focused on the self-pulsating operation of blue-emitting devices. Self-pulsation (SP) can significantly increase laser performance for certain applications and is considered, for example, to be important for the reduction of feedback noise [2]. In our previous work we have reported self-pulsation for a blue InGaN laser with a saturable absorber (SA) [3,4] and for tandem blue lasers [5]. The theoretical description of the device was based on the Yamada model for a laser with a SA [6,7] adapted to the specific case of a blue InGaN laser. In that work it was demonstrated that lasers with small carrier lifetime in the SA produced self-pulsation. The small carrier lifetime was attributed to piezoelectric and the tunnelling effects in the AlGaN layer, with the carrier recombination dominated by nonradiative processes.

Excitability is a rapidly expanding topic in optics, having been initially studied in biology [8] and chemistry [9]. Recently the phenomenon of excitability has been predicted to occur in optical devises such as cavities [10,12], different types of lasers [13-14] etc.. Convincing experimental evidence of excitability in a laser with a short external cavity is reported in [15]. In addition, an experimental investigation of the excitable properties of a solid-state laser with an intracavity saturable absorber is reported by Larotonda et al [16].

In this paper we present an investigation of self-pulsation and excitability in blue-violet lasers with different designs, which extends and complements our previous study of blue laser dynamics [3-5]. The structure of the paper is as follows: section 2 is devoted to a presentation of results on the InGaN laser with a SA incorporated as a layer parallel to the active region. Section 3 contains a presentation of the model, the associated equations, the results of simulations and a discussion of tandem blue lasers with different designs. The conclusions are given in Section 4.

2   Blue InGaN laser with saturable absorber

Fig. 1 shows the structure of the InGaN laser (lasing wavelength 395 nm) with saturable absorber that has been considered; it consists of a three-quantum well InGaN active layer and a saturable absorber in the form of a single p-type InGaN quantum well. Saturable absorber layers with thicknesses varying from 1 nm to 3 nm have been used with a view to maintaining a low threshold current. The AlGaN layer prevents significant carrier overflow from the active region. In the fabrication process, the saturable absorber layer was grown as a layer parallel to the active region. Other details of the fabrication method are given by Ohno et al [17]. The laser structure in Fig. 1 can be considered to be made up of a central active region 1 and a saturable absorber 2 as well as the outer regions 3 and 4. The other regions have been taken into account for the calculation of the effective refractive index, near field patterns and confinement factors. Region 5 is a cap layer, which is electrically connected to the external current source. The field distribution in the transverse cross-section is analyzed by the effective refractive index method, where the spatial variation of the refractive indices and 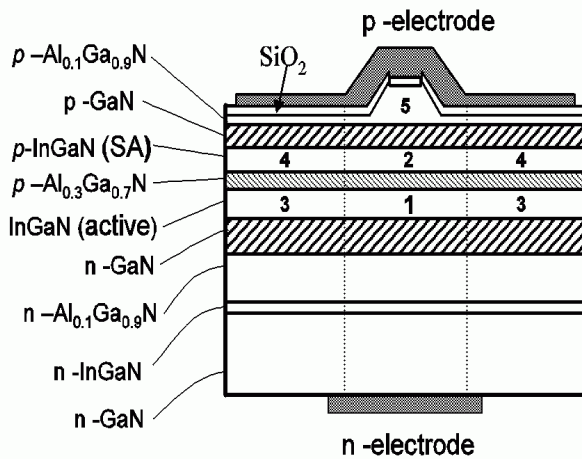the gain-loss properties of the media are taken into account. Each region of the device shown in Fig. 1 is taken to have a refractive index

Fig.1 Schematic view of the InGaN laser

that is dependent on its alloy composition and the wavelength of the radiation. The field confinement factors ξ_i of the regions 1 - 4 are not constant and have been evaluated during the pulsations. The equivalent volumes of the outer regions 3 and 4 also vary and were evaluated from the electron distribution width in these regions [7].

To model the laser properties, we used the Yamada model [6, 7] adapted to the specific case of the InGaN laser with saturable absorber incorporated as a layer parallel to active region. The equations of laser operation are

$$\frac{dS}{dt} = \left[\sum_i a_i \xi_i (N_i - N_{gi})/V_i - BS - G_{th} \right] S + M \sum_i a_i \xi_i N_i /V_i , \qquad (1)$$

$$\frac{dN_i}{dt} = -\frac{a_i \xi_i}{V_i}(N_i - N_{gi})S_i - \frac{N_i}{\tau_{si}} + \sum_{j \neq i}\left(\frac{N_j}{T_{ji}} - \frac{N_i}{T_{ij}} + \frac{(I_{ji} - I_{ij})}{e} \right), \qquad (2)$$

where S is the photon number, N_i is the injected carrier number in the ith region, a_i is the differential gain coefficient, ξ_i is the field confinement ratio, N_{gi} is the carrier number at transparency. τ_{si} is the carrier lifetime, T_{ij} is an equivalent lifetime giving the carrier diffusion from region j to i. I_{ij} gives the carrier injection from region j to i. The second term in the photon rate equation describes the spontaneous emission and M is the equivalent total number of longitudinal modes, which is evaluated from the half width of the linear gain spectrum. V_i is the volume expressed by $V_i = W_i d_i L$ where L is the laser length, and d_i and W_i are the thickness and width respectively of the relevant region. The term involving B describes the self-saturation of the gain and implies a nonlinearity of the system. The coefficient B is given by $B = B_c (N_1 - N_{g1})\frac{a_1 \xi_1^2}{V_1^2}$, where

$$B_c = \frac{9\pi c \tau_{in}^2 |R_{cv}|^2}{2\varepsilon_0 n_r^2 \hbar \lambda_0} \qquad (3)$$

and n_r is the refractive index, λ_0 is the central wavelength of the laser, R_{cv} is the dipole moment, and τ_{in} is the intraband relaxation time. The threshold gain level G_{th} is given by

$$G_{th} = \frac{c}{n_r}\left(\kappa + \frac{1}{2L}\ln\frac{1}{R_f R_B} \right), \qquad (4)$$

where R_f and R_b are the reflectivies of the front and the back facets, respectively and κ is the loss coefficient. The back facet has a high-reflection (HR) coating consisting of four pairs of quarter-wave TiO_2/SiO_2 dielectric multilayers to reduce the threshold current of the laser diodes, and we take R_f=0.25, R_b=0.95. The values of many of the above parameters are obtained from experimental measurements.

A typical example of a bifurcation diagram for periodic solutions is shown in Figure 2. A stability analysis shows that the limit cycle is created at a current of 125mA by a Hopf bifurcation (marked by a solid circle). This bifurcation diagram is completely different from that obtained in GaAs lasers that have been studied previously with a SA [6,18,19], where the self-pulsations appear just after the threshold due to a homoclinic bifurcation. In contrast, the bifurcation diagram in Figure 2 shows that a substantial region of CW operation exists after the threshold before SP occurs due to a Hopf bifurcation. Both Hopf bifurcation points in Figure 2 are subcritical. The carrier life time in the SA of the laser shown in Figure 1 was estimated from experiment to be about 0.1 ns, and this small value was attributed to piezoelectric and the tunnelling effects in the AlGaN layer, with the carrier recombination dominated by nonradiative processes. Our calculations show that the carrier lifetime in the SA strongly influences the bifurcation diagram. An increase of SA carrier lifetime shifts the lower Hopf point towards the threshold, and its bifurcation to a homoclinic one.
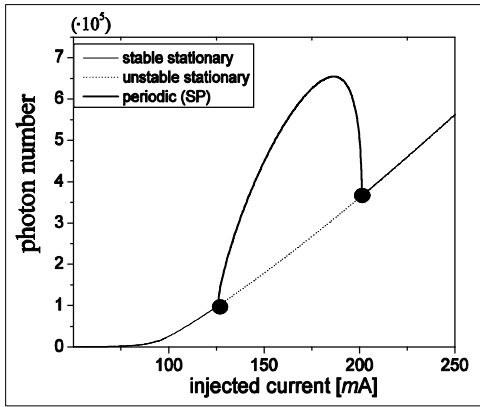

Fig.2 A bifurcation diagram for a laser with a 500 μm cavity length. The other parameters are as in Table 1. The thin solid lines show the stable stationary solutions (CW or non-lasing operation). The thin dotted line shows the unstable stationary solutions (SP operation). The thick solid line shows the periodic solutions. The circles mark the Hopf bifurcation points

Table 1   Parameters used in numerical calculations

Symbol	Definition	Value & units	
		Active region	SA
a	Differential gain coefficient	1.85×10^{-12} m^{3}s^{-1}	13.0×10^{-12}m^{3}s^{-1}
N_g	Transparency carrier density	1.4×10^{25}m^{-3}	2.6×10^{25}m^{-3}
τ_S	Carrier lifetime	2.0 ns	0.1 ns
d	Thickness	18nm	3 nm
W	Width	2.0μm	2.0μm

The region of self-pulsation in the plane of different parameters is shown in Figure 3. The first example is the SP region in the plane cavity length vs injected

current (Fig.3 a). For a laser with a small cavity length, the range of self-pulsation is narrow. As the cavity length is increased the SP range becomes wider. However, this spread is accompanied by a shift of the operating point to higher injected currents. We note that in the case of a laser with a 650 μm cavity length, the current injection was limited at 220mA due to the upper bias limit of the pulse current oscillator. Figure 3a also shows quite good agreement between the experimental data (dotted lines terminated by squares) and the regions of SP predicted by numerical calculation. The second example shows the influence of carrier lifetime on the laser dynamics. Fig 3b shows the SP region in the plane of carrier lifetime in the SA vs that of the active region for two values of SA thickness. This figure confirms once again the idea that a large carrier lifetime in the active region requires a short carrier lifetime in the SA to get self-pulsating operation. A decrease of SA thickness leads to the disappearance of the SP region. We found that in the case of a large carrier lifetime of the active region, SP operation can only be achieved with very small values of SA carrier lifetime.
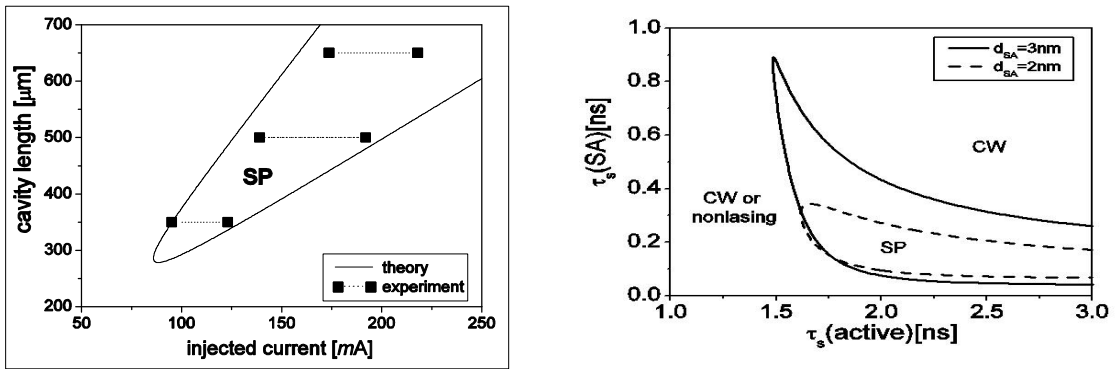

Fig. 3.a) The region of self-pulsation in the plane of cavity length vs. injected current. b) The region of self-pulsation in the plane of carrier lifetime in the SA vs. that in the active region for saturable absorber thicknesses of 2 nm and 3 nm. The cavity length is 500 μm and the injected current is 100mA. The lines denote the Hopf bifurcation points.

As was shown in [5], an approach to obtain excitability is to choose a suitable value for the absorption level in order to keep a low value for carrier lifetime in the SA. Fig. 4 shows a bifurcation diagram in the plane of SA differential gain coefficient versus injected current for a laser with a cavity length of 650 μm and carrier lifetimes of 2 ns and 0.5 ns in the active and SA regions respectively. For $a_{SA} < 12 \times 10^{-12} \, \text{m}^3 \text{s}^{-1}$ the laser shows either CW or non-lasing operation for any value of injected current. However, an increase of the differential gain coefficient of the SA causes the system to cross the Hopf-bifurcation line indicated by the solid thick line in Fig. 4. Further increase of the differential gain coefficient of the SA results in a homoclinic bifurcation, which is shown by the solid circle in Fig. 4. Between the dotted and

dashed lines, excitability is predicted to occur. The message from this figure is that to achieve excitability in practice by this approach we need a sufficiently high value of SA differential gain coefficient. However, increasing the SA differential gain coefficient increases both the absorption level and the injected current.
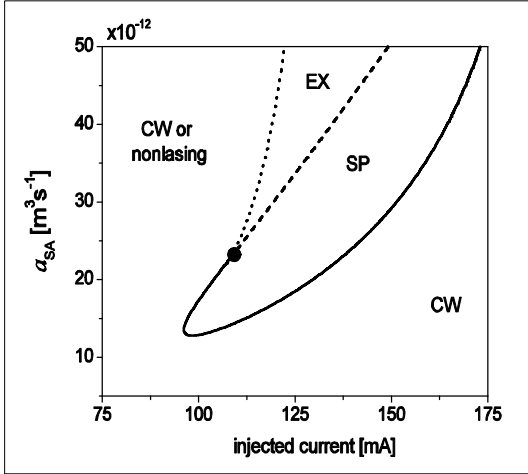

Fig.4. The bifurcation diagram in the plane of saturable absorber differential gain coefficient vs. injected current for a laser with a cavity length of 650 µm and a saturable absorber thickness of 2 nm. The carrier lifetimes in the active region and in the saturable absorber are 2 ns and 0.5 ns respectively. The other parameters are as in Table 1. The laser behaviour in the different regions is denoted by: excitable (EX), self-pulsating (SP) and CW or non-lasing. The solid line represents a Hopf bifurcation line.

3 Tandem blue lasers

Now we examine tandem InGaN lasers with different designs, which are shown schematically in Fig. 5 [5]. The devices consist of two regions, 1 and 2. Fig. 5(a) shows a laser in which both regions are active as a result of the two injected currents I_1 and I_2. In contrast, Fig. 5(b) shows a laser structure in which the region 1 is active while region 2 acts as a saturable absorber. Note that saturable absorber is grown next to the active region in the longitudinal direction, which is a completely different structure from that investigated in Section 2.
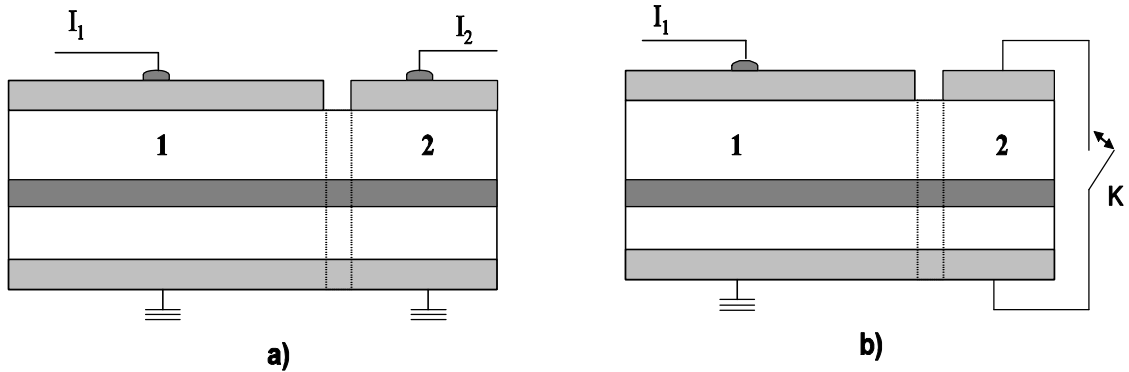

Fig. 5: Schematic illustration of the tandem blue-violet InGaN laser.

6

The laser dynamics have been investigated using the single mode rate equations

$$\frac{dS}{dt} = \left[\frac{L_1}{L} a_1 \xi_1 (n_1 - n_{g1}) + \frac{L_2}{L} a_2 \xi_2 (n_2 - n_{g2}) - G_{th}\right] S + M\left[a_1 \frac{L_1}{L} \xi_1 n_1 + a_2 \frac{L_2}{L} \xi_2 n_2\right] \quad (5)$$

$$\frac{dn_1}{dt} = -\frac{a_1}{V_1}\frac{L_1}{L}\xi_1(n_1 - n_{g1})S - \frac{n_1}{\tau_1} + \frac{I_1}{eV_1} \quad (6)$$

$$\frac{dn_2}{dt} = -\frac{a_2}{V_2}\frac{L_2}{L}\xi_2(n_2 - n_{g2})S - \frac{n_2}{\tau_2} + \begin{cases} \dfrac{I_2}{eV_2} & \mathrm{model}\ a \\ 0 & \mathrm{model}\ b\ K\ "open" \\ -\dfrac{n_2}{T_d} & \mathrm{model}\ b\ K\ "shut" \end{cases} \quad (7)$$

The subscripts 1 and 2 refer to regions 1 and 2, respectively; $n_{1(2)}$ is the injected carrier density. T_d is the effective diffusion lifetime induced by the shutting of switch K. The other notations are kept as in (1)-(4). However, the refractive index from (4) is calculated by the first-order Sellmeier equation $n_r = \sqrt{b_1 + \lambda^2/(\lambda^2 - b_2)}$, where b_1 and b_2 are the fitting parameters ($b_1 = 4.37$ and $b_2 = 8.76 \times 10^4$ m^2). The parameters values $\kappa = 20$ cm^{-1}, $a_1 = 1.5 \times 10^{-12}$ m^{3}s^{-1}, $a_2 = 9.0 \times 10^{-12}$ m^{3}s^{-1}, $\tau_{S1} = 1$ns, ridge width 2μm, and active regions thickness 16nm were used for calculating the results that are shown in figures 6-8.

We consider three cases determined by the injected current I_2 and the position of the switch K for the devices in Fig. 5. The first case is the configuration shown in Fig. 5a where injected currents are supplied to the regions 1 and 2. In this case both regions are active. The results are shown in fig. 6 where the current injected into region 2
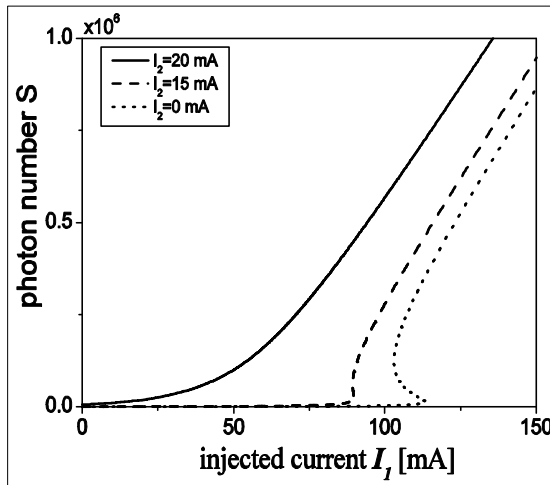

Fig. 6: The stationary dependence of photon number S on the current injected into region 1 for different values of the current injected into region 2 (Fig.5a). The cavity lengths are 500μm and 200μm for regions 1 and 2, respectively. The other parameters used in the calculations are: $n_{g1} = 1.8 \times 10^{25}$ m^{-3}, $n_{g1} = 1.0 \times 10^{25}$ m^{-3}, $\tau_{S2} = 1.0$ns.

varies from 0 up to 20 mA. For no current supply to region 2, the calculations predict that there is hysteresis in the stationary dependence of photon number S on the injected current of region 1. In this case the experimental data show that switching occurs but pulsation does not. As the injected current in region 2 is increased, the threshold current of region 1 is lowered and the hysteresis disappears. For a 20mA current injected into region 2, the threshold current of region 1 is reduced to 50mA. However, only CW operation can be achieved in this case.

Now consider the second case where the switch K of Fig.5b is closed, so that there is carrier transport through it and a consequent reduction of the carrier life time in region 2. As was mentioned previously, the reduction of carrier life time in the SA can result in the appearance of self-pulsating operation. The region of SP in the plane region 2 cavity length vs. injected current of region 1 for two values of carrier life time of region 2 is plotted in Figure 7. For a 0.1ns carrier lifetime in region 2, the region of SP is wide and is in a good agreement with the experimental data marked by the dashed line terminated by solid squares. Increasing the carrier lifetime of region 2 makes the SP region smaller and shifts it to higher cavity lengths (dotted line in Fig. 7).

The above results provide clear evidence of the presence of hysteresis and the first indication that the phenomenon of excitability might be possible. Now, we will focus on the study of the laser behaviour in the case when the switch K of Fig.5b is open.
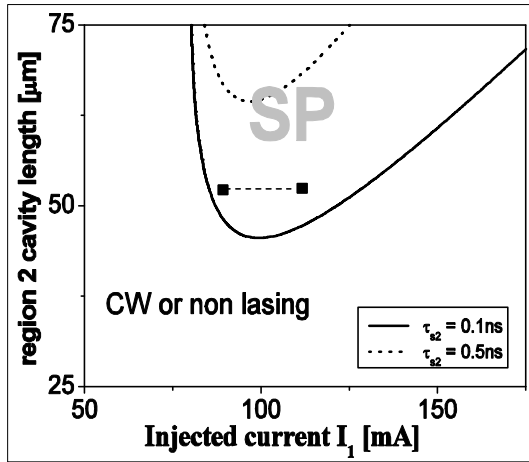

Fig.7: The region of self-pulsation in the plane of cavity length vs. injected current of region 1 for different values of carrier lifetime in the region 2. The parameters are $\tau_{S2} = 0.1ns$, $T_d = 0.1ns$, $a_1 = 1.5\times10^{25}m^3s^{-1}$, $a_1 = 9.0\times10^{25}m^3s^{-1}$, $\xi_1 = 0.05$, $\xi_2 = 0.02$, $n_{g1} = 2.3\times10^{25}m^{-3}$, $n_{g1} = 2.3\times10^{25}m^{-3}$ and $L_1 = 490\mu m$. The dotted line terminated by squares shows the range of self-pulsation observed experimentally.

Figure 8 shows the bifurcation diagram in the plane region 2 cavity length vs. injected current of region 1. The solid line shows the Hopf bifurcation points and is terminated by a saddle node bifurcation marked by a solid circle. A linear stability analysis shows that in the region EX a node, a saddle and an unstable focus coexist and the system behaves as an excitable one. The numerical calculations also confirm the

8

three characteristics of excitability: the existence of a threshold above which an excitation can occur; a response independent of the magnitude of a perturbation above threshold; and the existence of a refractory period.
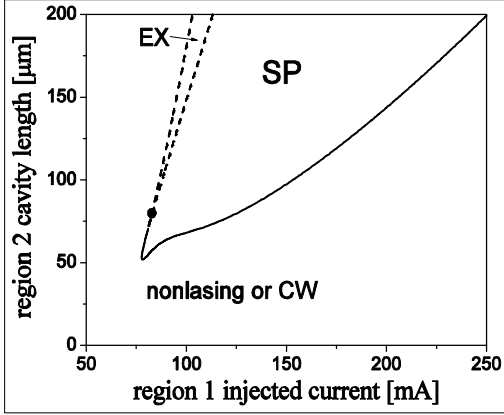

Fig. 8 Bifurcation diagram in the L_2 - I_1 plane when the switch K in Fig. 5b is open. The parameters are $L_1 = 500\mu m$, $n_{g1} = 1.8 \times 10^{25} m^{-3}$, $n_{g1} = 1.0 \times 10^{25} m^{-3}$, $\tau_{S2} = 1.0 ns$. The circle denotes the point of saddle node bifurcation.

Although the experimental achievement of excitable behaviour in InGaN lasers is unlikely to be straightforward, it should be possible in practice to observe excitability both in lasers with a large cavity length and a saturable absorber incorporated as a layer parallel to the active region, and also in tandem lasers. We believe that our work provides a good basis for future study and, in particular provides some pointers for more detailed investigations of excitability, and the associated phenomenon of coherence resonance, in InGaN lasers and of their possible practical applications.

4. Summary and conclusions

In this paper we have investigated the CW, self-pulsating and excitable behaviour of blue-violet InGaN lasers with different designs. The ways in which the properties of the SA determine the laser output characteristics have been considered. It was found that a short carrier lifetime in the SA is conducive to SP while lasers with a large SA carrier lifetime are more suited to excitability. Also, we have shown that an increase of SA absorption level leads to the appearance of a homoclinic bifurcation and can result in excitability. For tandem lasers, an injected current into one region produces a low threshold current in the other but results only in CW operation. However, self-pulsating operation of tandem InGaN lasers is possible with an external circuit. Finally, we have presented a bifurcation diagram, which suggest that excitability in tandem InGaN lasers is possible.

Acknowledgments

REFERENCES

[1] S. Nakamura, S. Pearton, and G. Fasol, The Blue Laser Diode, 2nd ed. Springer, Berlin, 2000.

[2] M.Yamada, "A theoretical analysis of quantum noise in Semiconductor laser operating with self-sustained pulsations, "IEICE Transactions on Electronics, E81-C pp. 290-298, 1998.

[3] V.Z.Tronciu, M.Yamada, Tomoki Ohno, Shigetoshi Ito, Toshiyuki Kawakami, and Mototaka Taneya. "Self-pulsation in an InGaN laser - theory and experiment", IEEE J. Quantum Electronics. Vol. 39, No 12 pp 1509-1514, 2003.

[4] V.Z.Tronciu, Minoru Yamada, and R.A.Abram "Analysis of the dynamics of a blue-violet InGaN laser with saturable absorber" submitted Phys Rev E 2004.

[5] V.Z.Tronciu, M.Yamada Toshiyuki Kawakami, Shigetoshi Ito, Tomoki Ohno Mototaka Taneya and R.A.Abram "The theoretical and experimental investigation of the dynamics of tandem blue-violet lasers" Optics Communications Vol 235/4-6 pp 409-414 (2004)

[6] M.Yamada, "A theoretical Analysis of self- sustained pulsation phenomena in narrow- stripe semiconductor lasers" IEEE J. Quantum Electron., 29, pp. 1330-1336, 1993.

[7] M.Yamada M. Yamada, IEICE Trans. Electron. **E8**1-C, 290 (1998).

[8] J.D. Murray, *Mathematical Biology*, Springer 1990.

[9] S.Grill, V.S.Zykov, and S.C.Mueller, *J.* Phys. Chem. 100, 19082 (1996).

[10] W.Lu, D.Yu, and R.G. Harrison Phys. Rev. *A* 58(2), R809 (1998).

[11] V.Z.Tronciu and R.A.Abram "Excitability of excitons and biexcitons in a ring cavity", Phys. Rev. E., 65 p. 026616, 2002.

[12] J.L.A.Dubbeldam, B.Krauskopf, and D.Lenstra, Phys. Rev. E 60(6), 6580, 1999.

[13] M.Giudici, C. Green, G. Giacomelli, U. Nespolo, J. R. Tredicce, Phys. Rev. E 55, 6414, 1997; M.Giudici, C. Green, G. Giacomelli, U. Nespolo, J. R. Tredicce, Phys. Rev. E 58, 4043, 1998; Van Tartwijk G.H.M., I. Fischer, Phys. Rev. E 58 4041 1998; Viktorov E.A., P. Mandel, Phys. Rev. Lett. **85** 3157 (2000); Tredicce J.R. *AIP Conference Proceedings*, 548 238, 2000.

[14] V.Z.Tronciu, H.J.Wünsche, K Schneider and M.Radziunas, "Excitability of lasers with integrated dispersive reflector" SPIE Proceedings 4283 347-354, 2001.

[15] H.J.Wünsche, O.Brox, M.Radziunas and F.Henneberger, "Excitability of a Semiconductor Laser by a Two-Mode Homoclinic Bifurcation" Phys.Rev.Lett. 88 023901, 2002

[16] M.A. Larotonda, A.Hnilo, J.M.Mendez,A.M Yacomotti Phys.Rev. A 65, 033812 2002

[17] T.Ohno, S.Ito, T. Kawakami and M.Taneya, "Self- pulsation in InGaN laser diodes with saturable absorber layers," Appl. Phys. Lett. 83, 1098, 2003

[18] J. L. A. Dubbeldam and B. Krauskopf, "Self-pulsations of lasers with saturable absorber: Dynamics and bifurcations," *Opt. Commun.*, vol. 159, pp. 325–338, 1999.

[19] C. R. Mirasso, G. H. M. van Tartwijk, E. Hernandez-Garcia, D. Lenstra, S. Lynch, P. Landais, P. Phelan, J. O'Gorman, M. S. Miguel, and W.Elsaer, "Self-pulsating semiconductor lasers: Theory and experiment," *IEEE J. Quantum Electron.*, vol. 35, pp. 764–770, 1999.